JOBNAME: JCLI 00#00 2021 PAGE: 1 SESS: 8 OUTPUT: Tue Apr 6 06:10:18 2021 Total No. of Pages: 18
/ams/jcli/0/jcliD200308

Diurnal Cycle of Coastal Convection in the South China Sea Region and Modulation by the BSISO

WEIXIN XU,[a,b,c] STEVEN A. RUTLEDGE,[d] AND KYLE CHUDLER[d]

[a] *Sun Yat-Sen University, Zhuhai, China*
[c] *Guangdong Province Key Laboratory for Climate Change and Natural Disaster Studies, Guangzhou, China*
[d] *Southern Marine Science and Engineering Guangdong Laboratory (Zhuhai), Zhuhai, China*
[b] *Colorado State University, Fort Collins, Colorado*

(Manuscript received 30 April 2020, in final form 6 January 2021)

ABSTRACT: Using 17-yr spaceborne precipitation radar measurements, this study investigates how diurnal cycles of rainfall and convective characteristics over the South China Sea region are modulated by the boreal summer intraseasonal oscillation (BSISO). Generally, diurnal cycles change significantly between suppressed and active BSISO periods. Over the Philippines and Indochina, where the low-level monsoon flows impinge on coast lines, diurnal cycles of rainfall and many convective properties are enhanced during suppressed periods. During active periods, diurnal variation of convection is still significant over land but diminishes over water. Also, afternoon peaks of rainfall and MCS populations over land are obviously extended in active periods, mainly through the enhancement of stratiform precipitation. Over Borneo, where the prevailing low-level winds are parallel to coasts, diurnal cycles (both onshore and offshore) are actually stronger during active periods. Radar profiles also demonstrate a pronounced nocturnal offshore propagation of deep convection over western Borneo in active periods. During suppressed periods, coastal afternoon convection over Borneo is reduced, and peak convection occurs over the mountains until the convective suppression is overcome in the late afternoon or evening. A major portion (>70%) of the total precipitation over the Philippines and Indochina during suppressed periods falls from afternoon isolated to medium-sized systems (<10 000 km^2), but more than 70% of the active BSISO rainfall is contributed by nocturnal (after 1800 LT) broad precipitation systems (>10 000 km^2). However, offshore total precipitation is dominated by large precipitation systems (>10 000 km^2) regardless of BSISO phases and regions.

KEYWORDS: Convection; Madden-Julian oscillation; Mesoscale systems; Diurnal effects; Precipitation; Intraseasonal variability

AU1

1. Introduction

During boreal summer, the Asian monsoon produces copious rainfall and strongly influences regional and global atmospheric circulations (Wang 2006). Coupled to the mean Asian summer monsoon (ASM) flow and its rainfall is the boreal summer intraseasonal oscillation (BSISO; Wang and Xie 1997; Waliser 2006; DeMott et al. 2013; Lee et al. 2013). Whereas its boreal winter counterpart (October–April), the Madden–Julian oscillation (MJO), is dominated by eastward propagation in the tropics, the BSISO (May–September) propagates eastward and northward (Wang and Xie 1997; Kemball-Cook and Wang 2001; Jiang et al. 2004). The BSISO has two modes, including the 30–60-day (similar to the MJO) and the 10–20-day oscillations (Wang 2005; Waliser 2006; Kikuchi et al. 2012; Lee et al. 2013). The dominant 30–60-day mode of the BSISO features a northwest–southeast tilted rainband between the Bay of Bengal and the South China Sea (SCS) during the active period (Wang and Xie 1997). BSISO anomalies substantially reduce the mean low-level southwesterly/westerly flow and precipitation of the monsoon during the suppressed phases, but strongly enhance the monsoonal winds and rainfall during active phases (Wang and Xie 1997; Waliser 2006; Lee et al. 2013; Xu and Rutledge 2018).

On a smaller scale, the BSISO significantly modulates mesoscale organization, cloud vertical structure, precipitation microphysics, and lightning activity over the Bay of Bengal (BOB), the SCS, the western tropical Pacific Ocean, and the Maritime Continent (Ho et al. 2008; Virts and Houze 2016; Xu and Rutledge 2018; Chudler et al. 2020). In the Indian monsoon region, active BSISO periods are conducive to large mesoscale convective systems (MCSs; >41 000 km^2) and lightning activities, although they are not in phase over a specific location (Virts and Houze 2016). Xu and Rutledge (2018) showed that during active BSISO phases the frequency of shallow cumulus decreases while convective upscale growth and stratiform precipitation are enhanced due to increased vertical shear and moister midlevels. However, intensity of land-based convection substantially weakens after the BSISO onset (Ho et al. 2008; Xu and Rutledge 2018; Chudler et al. 2020). For instance, land-based convection has a stronger microwave ice scattering signature, deeper and more intense radar structures, and larger lightning flash rates during suppressed BSISO phases than active phases. Xu and Rutledge (2018) proposed that these convective variabilities may be attributed to greater convective instability and a stronger diurnal cycle under a calmer, less cloudy, and drier surface conditions during the suppressed periods.

Many studies have investigated the diurnal cycles of rainfall over the SCS (Aves and Johnson 2008) and surrounding areas

Supplemental information related to this paper is available at the Journals Online website: https://doi.org/10.1175/10.1175/JCLI-D-20-0308.1.s1.

Corresponding author: Weixin Xu, xuwx25@mail.sysu.edu.cn

DOI: 10.1175/JCLI-D-20-0308.1

JOBNAME: JCLI 00#00 2021 PAGE: 2 SESS: 8 OUTPUT: Tue Apr 6 06:10:18 2021 Total No. of Pages: 18
/ams/jcli/0/jcliD200308

including the Philippines (Ho et al. 2008; Natoli and Maloney 2019; Chudler et al. 2020), the Indochina Peninsula (Takahashi et al. 2010), southern China (Chen et al. 2019), and the Maritime Continent (MC; Houze et al. 1981; Ichikawa and Yasunari 2006, 2007; Kanamori et al. 2013; Peatman et al. 2014; Sakaeda et al. 2017). Generally, the diurnal cycle over land shows maximum afternoon rainfall due to onshore sea breezes and local surface heating, whereas nocturnal rainfall dominates offshore and in coastal areas. Nocturnal rainfall maxima were also observed near the base of mountain ranges where downslope drainage winds collide with the prevailing onshore large-scale airflow (Takahashi et al. 2010). Several mechanisms may be responsible for the nocturnal offshore or coastal rainfall maxima in the SCS region. First of all, convergence between the nighttime land breezes and onshore low-level monsoon flow may significantly enhance precipitation (Houze et al. 1981; Ichikawa and Yasunari 2006). The nocturnal land breeze could be further enhanced by the katabatic drainage winds from coastal mountain ranges (Ruppert et al. 2013). Second, Xu et al. (2012) showed that heavy offshore precipitation occurs when low-level southwesterly monsoon flow is lifted by precipitation-generated cold pools extending well offshore from southwestern Taiwan. Xu et al. showed that precipitation cold pools persist for a fairly long time period (>12 h), continually fed by evaporative cooling of precipitation, pushed by strong low-level upstream flows, and blocked by downstream mountain ranges (Xu et al. 2012). Last but not least, a gravity wave mechanism proposed by Mapes et al. (2003) was offered to explain some of the offshore propagating convection. For instance, gravity wave forced lower troposphere cooling was observed offshore of western Sumatra (Yokoi et al. 2017). Aves and Johnson (2008) attributed the gravity wave mechanism to explain why convection frequently initiates off the southern China coast and propagates southeastward, extending 500 km offshore. In fact, this offshore propagation of convection resembles the discrete nature of gravity waves. Yokoi et al. (2017) showed that offshore propagation of the afternoon land-based convection occurs mainly under the presence of significant vertical wind shear. Although the diurnal cycle of convection in the SCS region has been examined in detail, how it interacts with the BSISO is not understood.

Previous studies demonstrated that the MJO substantially modulates the magnitude and phase of the diurnal cycle of rainfall in the MC. The amplitude of the rainfall diurnal cycle over land is generally enhanced during suppressed MJO phases versus active phases (Sui and Lau 1992; Rauniyar and Walsh 2011), while the phase of the rainfall diurnal cycle is delayed during MJO active periods (Rauniyar and Walsh 2011; Sakaeda et al. 2017). Also, the diurnal convective disturbances propagate farther offshore during active phases (Rauniyar and Walsh 2011; Sakaeda et al. 2017). Rainfall diurnal cycle over MC islands tends to peak several days before the arrival of the broad MJO convective envelope (Sui and Lau 1992; Ichikawa and Yasunari 2007; Kanamori et al. 2013; Peatman et al. 2014). Prior to the MJO onset, conditions of limited cloudiness, strong surface insolation, and light winds may collectively act to promote strong land–sea breeze circulations. The increasing instability and tropospheric moistening during this period, along with enhanced land–sea breezes, induce greater variability in diurnal precipitation (Peatman et al. 2014; Birch et al. 2016; Vincent et al. 2016). Ichikawa and Yasunari (2007) showed that the direction of the offshore propagating diurnal disturbances shifts from westward to eastward during the passage of the MJO over the MC, which may feed back to the overall propagation of the MJO. Lightning demonstrates similar behavior in response to the MJO; for example, the diurnal cycle of lightning is amplified over western Borneo during suppressed MJO periods but enhanced to the east (leeward) of major mountains in MC during active MJO phases (Virts et al. 2013). Nevertheless, regional models have only limited ability to realistically simulate interactions between the MJO and the diurnal cycle over the MC (Birch et al. 2016; Vincent et al. 2016).

Interactions between the BSISO and diurnal cycle in the SCS region have not been subject to extensive study. Ho et al. (2008) showed that rainfall over the SCS maximizes just off the western Philippine coast, and the rainfall maximum shifts from late evening during the suppressed BSISO to the late morning during active BSISO. They suggested that the evening peak rainfall in the suppressed BSISO period originates from the offshore propagating land-based afternoon convection, whereas the morning offshore rainfall maximum is due to extension of organized mesoscale convective systems by local convergence along the coast during active BSISO. Natoli and Maloney (2019) found that the amplitude of the rainfall diurnal cycle over Luzon as well as offshore propagation peaks just prior to the BSISO onset and minimizes during the transition from active to suppressed BSISO periods. Using over 20 years of spaceborne precipitation radar data, Chudler et al. (2020) investigated how the BSISO influences the diurnal variability of precipitation, convective intensity, and morphology offshore and over Luzon. They found a pronounced diurnal cycle of convection over Luzon through the BSISO life cycle, even during active BSISO phases when solar heating and instability are apparently reduced due to enhanced cloud cover. The diurnal cycle of offshore precipitation weakens during active phases, and precipitation systems persistently occur over the ocean in terms of both isolated and organized broad systems. The underlying mechanism may be associated with increases in surface heat fluxes, increased vertical wind shear, and enhanced convergence of the monsoon flow with higher terrain during active BSISO periods (Ogura and Yoshizaki 1988; Xie et al. 2006). Chen et al. (2019) showed that both rainfall diurnal cycle and mean precipitation rate of coastal southern China are strongly enhanced during the convectively suppressed phases over the SCS (e.g., BSISO phase 1). They also found that offshore rainfall exhibits the greatest diurnal variability at the end of the BSISO active phase (e.g., phase 8). The changes in the diurnal cycle over southern China are possibly induced by the interaction between the larger-scale BSISO associated anomalous moisture advection and the local land–sea breeze circulations (Chen et al. 2019).

Although rainfall diurnal variations in the SCS region have been previously investigated, many details in the diurnal cycle of coastal convection and its relationship with the BSISO remain unanswered. First of all, the influence of the BSISO on the diurnal cycle throughout the SCS is not well known. Second, previous studies mainly used satellite rainfall estimates based on passive remote sensing techniques, which are generally less

JOBNAME: JCLI 00#00 2021 PAGE: 3 SESS: 8 OUTPUT: Tue Apr 6 06:10:18 2021 Total No. of Pages: 18
/ams/jcli/0/jcliD200308

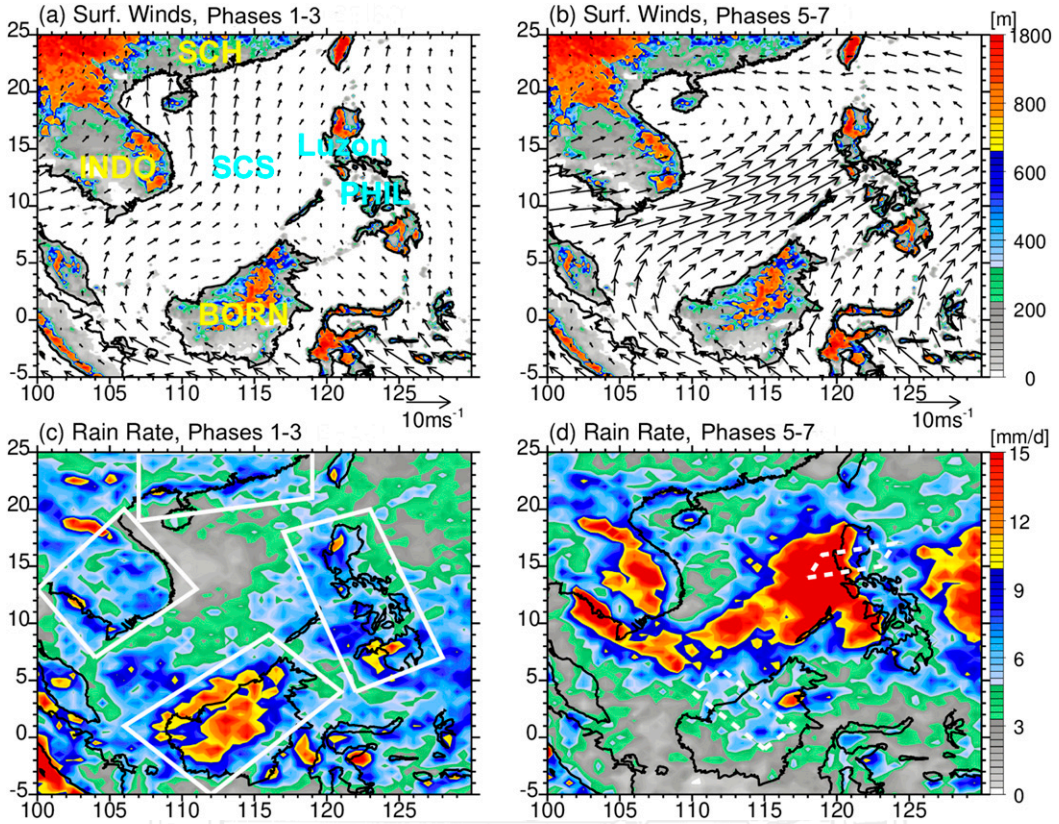

FIG. 1. (a),(b) CCMP surface winds (arrows) overlay the terrain elevation (color shaded), and (c),(d) TRMM PR-based mean rain rate, during phases 1–3 and 5–7. White solid boxes in (c) mark specific study regions, and white dashed strips in (d) indicate vertical cross-section locations. Main locations referred in this study are labeled in (a), including "SCS" (South China Sea), "SCH" (Southern China), "Luzon", "PHIL" (Philippines), "BORN" (Borneo), and "INDO" (Indochina).

accurate especially when infrared data are used (Gopalan et al. 2010; Kummerow et al. 2015). This study will use spaceborne precipitation radar measurements instead. Also, most diurnal cycle research focused on the surface rainfall statistics but rarely investigated convective characteristics such as precipitation type, vertical structure, mesoscale organization, convective intensity, and lightning activity, which are major objectives of this study. Last but not least, tropical cyclone precipitation was not excluded from the monsoon rainfall. Tropical cyclone precipitation contributes a large portion (up to 30%–40%) of the seasonal rainfall in the SCS region (Jiang and Zipser 2010). This study will examine the variability (regional and intraseasonal) in the diurnal cycle of precipitation over the SCS and surrounding landmasses using 17 years of spaceborne radar observations. The diurnal variations of the mesoscale structures and convective characteristics of precipitating systems and how they change during suppressed and active phases of the BSISO will be further investigated.

2. Data and methodology

This study uses 17 years (1998–2014) of spaceborne precipitation radar measurements, satellite-based lightning observations, precipitation feature data, and multisatellite wind retrievals to investigate diurnal cycles of surface rainfall, flow patterns, and convective structures. These data are stratified by the BSISO phase index (Lee et al. 2013). This study focuses on the key BSISO region over the SCS and surrounding landmasses (5°S–25°N, 100°–130°E), including the Philippines, the Indochina Peninsula, Borneo, and Southern China as marked in Fig. 1 (consistent with Xu and Rutledge 2018).

a. *Multisatellite wind retrievals*

NASA's Cross-Calibrated Multi-Platform (CCMP) ocean surface wind vector analysis product (Atlas et al. 2011) is used to study the diurnal cycle of surface winds. The CCMP dataset utilizes a variational analysis method to combine multiple satellite wind retrievals from radiometers/scatterometers, wind measurements from moored buoys, and wind reanalysis data from the European Centre for Medium-Range Weather Forecasts interim reanalysis (ERA-Interim) database. Satellite radiometer and scatterometer wind retrievals are validated against ocean moored buoys for consistency. Global CCMP winds are referenced to a height of 10 m with a 0.25° horizontal resolution and are available at 6-h intervals from 1987 onward. In this study, the 6-h CCMP

JOBNAME: JCLI 00#00 2021 PAGE: 4 SESS: 8 OUTPUT: Tue Apr 6 06:10:18 2021 Total No. of Pages: 18
/ams/jcli/0/jcliD200308

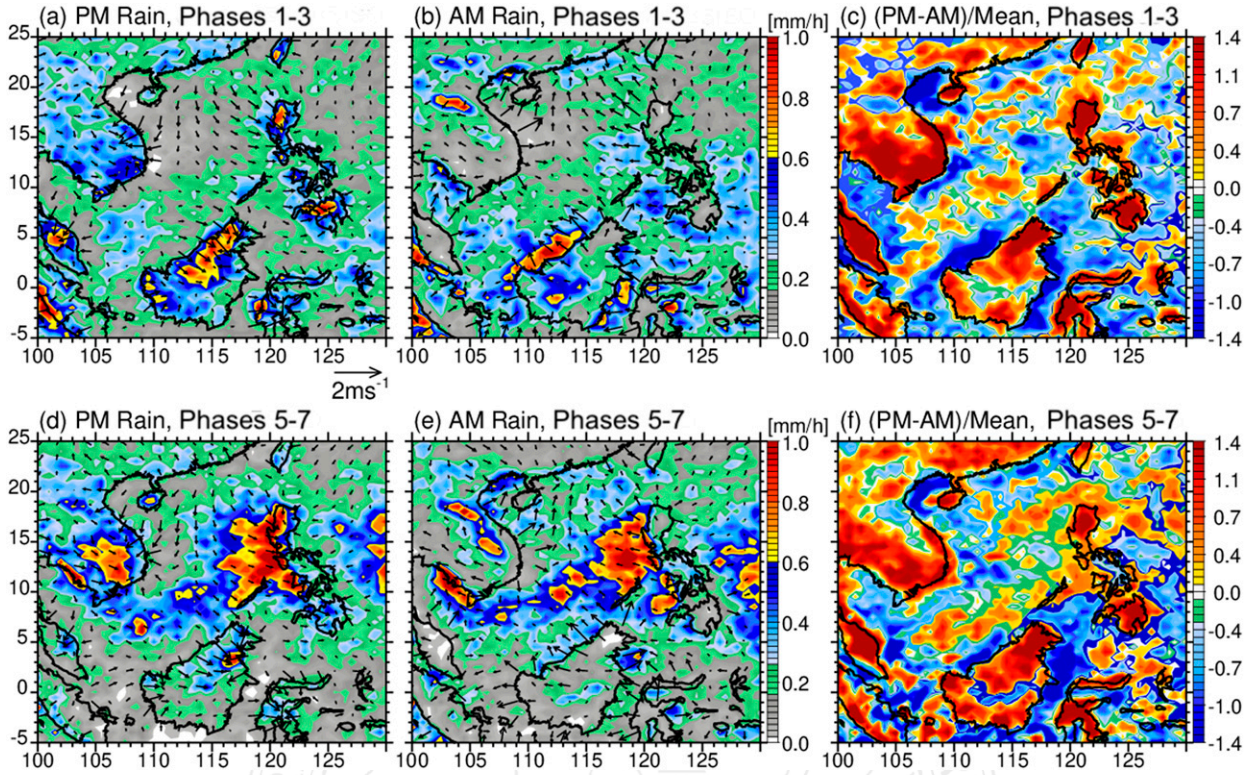

FIG. 2. TRMM PR-based mean rain rate during the PM hours (1200–2300 LT) and AM hours (0000–1200 LT) during phases (a),(b) 1–3 and (d),(e) 5–7, and the normalized difference between the PM and AM (PM − AM) rain rates (divided by daily mean rain rate) for phases (c) 1–3 and (f) 5–7). Arrows represent the CCMP surface wind anomalies from daily mean.

data are linearly interpolated into 3-h wind fields for comparison with the rain-rate field.

b. *Spaceborne radar measurements*

Two different levels of Tropical Rainfall Measuring Mission (TRMM) precipitation radar (PR) data are utilized, specifically, the PR 2A25 orbital data (Iguchi et al. 2000) and the precipitation feature (PF) database from the University of Utah (Liu et al. 2008), both in version 7. First of all, all the PFs and PR orbital data related to tropical cyclone (TC) passage are excluded by removing data within 500 km of TC centers based on TC best track data from the International Best Track Archive for Climate Stewardship (Knapp et al. 2010). Surface rain rates, precipitation type (convective vs stratiform), and composited vertical cross sections are derived from the PR orbital data. The original 5-km-resolution PR data are interpolated (average point method) into 50-km-resolution grids and composited into eight 3-hourly periods from 1998 to 2014. Rain rates are also calculated separately for convective and stratiform precipitation type. There are ample PR samples during 17 years for diurnal study; for example, each 50-km grid includes nearly 15 000 PR samples (pixels; see Fig. S1 in the online supplemental material) in a composited 3-h period during 1998–2014. We use the original PR vertical profiling data, which have a vertical resolution of 250 m, to calculate the frequency of convective occurrence in a composited vertical cross section. Basically, one PR surface sample corresponds to one vertical radar profile from the near surface up to 20 km. Vertical PR profiles within a cross section are combined to derive the frequency of radar echo as a function of distance (from the coast) and height.

The PF database is used to derive diurnal variations on organization and maximum convective depth of precipitation systems. The PF technique classifies clusters of PR near-surface raining pixels (5-km horizontal resolution) as PFs. The centroid of the cluster is defined as the PF location using an elliptical fitting technique. Measurements from various sensors (e.g., radar, microwave, and lightning) with different spatial resolutions are then collocated into common grids (5-km resolution) within each PF. The PF database provides many precipitation and cloud quantities of precipitation systems including precipitation area (size) and volume, maximum height of certain radar reflectivity thresholds (e.g., 20 dBZ), microwave ice scattering signatures, lightning flash rates, etc. In this study, frequencies of deep convection (20-dBZ echo-top height > 12 km) and organized MCSs (PF area > 2000 km^2), as well as rainfall (rain volume) contribution relative to size (PF area), are derived from the PF database.

c. *Satellite-based lightning observations*

Lightning (flash) densities are calculated using lightning measurements from the TRMM Lightning Imaging Sensor (LIS,

JOBNAME: JCLI 00#00 2021 PAGE: 5 SESS: 8 OUTPUT: Tue Apr 6 06:10:19 2021 Total No. of Pages: 18
/ams/jcli/0/jcliD200308

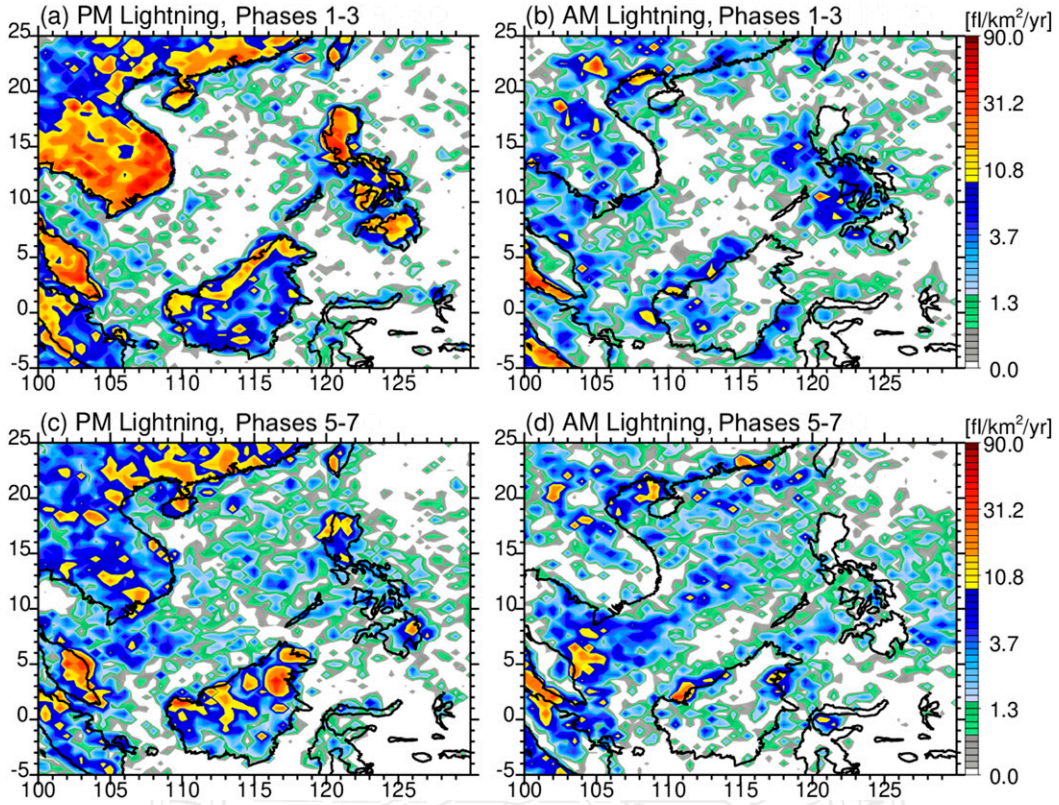

FIG. 3. TRMM LIS-based lightning density in the PM (1200–2300 LT) and AM (0000–1200 LT) during phases (a),(b) 1–3 and (c),(d) 5–7. Color shading and color bar is in a log scale.

version 7). LIS flash data from all orbits overpassing the study region are used. During each TRMM overpass, LIS detects radiance from lightning flashes in 5-km-horizontal-resolution and 2-ms-temporal-resolution bins (Christian 1999). Total lightning events (intracloud and cloud-to-ground lightning) are first derived through separating the lightning radiance from the background radiance by the LIS algorithm (Christian 1999). Lightning flashes are further identified as clusters of optical events with spatial separation less than 5.5 km and a temporal interval shorter than 330 ms. The LIS flash detection efficiency has been estimated to be 70% during the day and up to 90% at night (Boccippio et al. 2002; Christian et al. 2003). Flash density is calculated as total number of flashes divided by LIS total sampling time within a grid (50-km resolution). Since TRMM LIS has a broader observing swath than PR (650 vs 250 km), the area of LIS sampling is much greater compared to PR.

d. BSISO indices and definitions

The major goal of this study is to examine the differences in diurnal patterns of convection between suppressed and active BSISO periods. For this purpose, the real-time nonfiltering Lee et al. 2013 index (herein the L13 index; http://iprc.soest.hawaii.edu/users/jylee/bsiso) is utilized, which may better capture diurnal variability. Basically, multivariate empirical orthogonal functions (MV-EOFs) of 850-hPa zonal wind and outgoing longwave radiation over the ASM region (10°S–40°N, 40°–160°E) are applied (without any bandpass filtering) to derive the L13 index. This study analyzes the 30–60-day mode of the BSISO, which is represented by the first and second EOF principal components (PCs). To focus on major BSISO conditions, only days (during June–September) with significant BSISO amplitude are included; that is, $(PC1^2 + PC2^2)^{1/2} > 1$. The phase-by-phase evolution of the rainfall map (Fig. 2 in Xu and Rutledge 2018) shows that the pronounced northwest–southeast-oriented rainband of the active BSISO over the SCS, Indochina, and the Philippines occurs in phases 5–7, which are defined as "active" BSISO periods over these regions. In contrast, precipitation is the most suppressed during phases 1–3, which are classified as their "suppressed" BSISO periods. On the other hand, Borneo and Southern China nearly have opposite suppressed/active phases as the key BSISO regions (the SCS, Indochina, and the Philippines), as pointed out by Xu and Rutledge (2018). Further discussion on this point will be provided in section 3a. As such, the "active" and "suppressed" periods of Borneo and southern China are defined by phases 1–3 and phases 5–7, respectively. There are ample data samples in both suppressed and active BSISO periods (amplitude > 1), including more than 500 sample days with over 3000 TRMM overpasses in each period, providing confidence for the period composites in this study.

Historical BSISO indices are typically derived through applying a 25–90-day bandpass filter to the outgoing longwave radiation

JOBNAME: JCLI 00#00 2021 PAGE: 6 SESS: 8 OUTPUT: Tue Apr 6 06:10:19 2021 Total No. of Pages: 18
/ams/jcli/0/jcliD200308

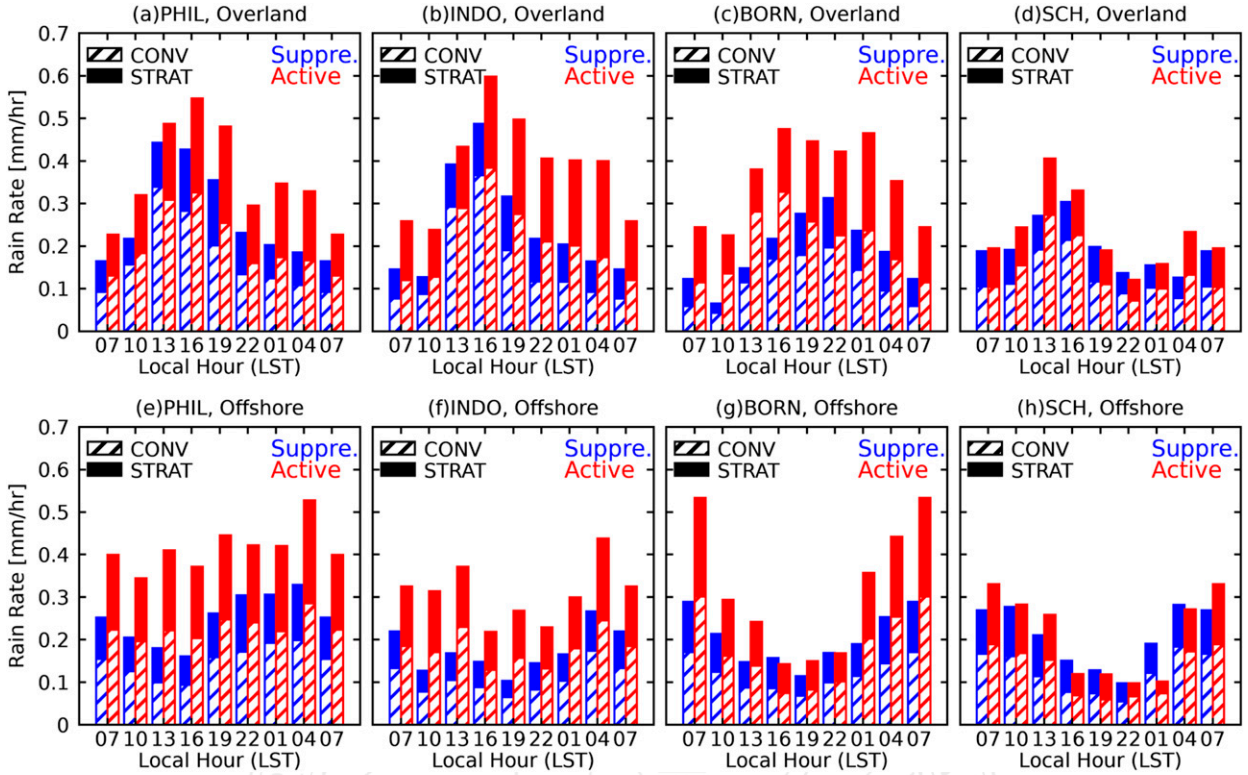

FIG. 4. Time series of PR-based 3-hourly areal mean rain rates separated into convective (hatched) and stratiform (filled) rain types for (a)–(d) overland and (e)–(h) offshore areas of selected regions (marked in Fig. 1c) during their suppressed (blue bars) and active (red bars) BSISO periods.

(OLR) and *U*-wind component at 850 hPa (U850) fields, so that the BSISO propagation could be better represented (Kiladis et al. 2014; Wang et al. 2018). Statistical tests have been conducted using the L13 index and the filtered OLR MJO index (OMI; Kiladis et al. 2014; Wang et al. 2018). First of all, the L13 and OMI indices agree on active/suppressed phases most of the time (80%) and rarely indicate opposite phases. Most of the difference comes when L13 classifies active or suppressed phase, and the OMI indicates the same phase but with an amplitude < 1. As a result, the OMI-based convective samples (292 879 PFs) are ~20% smaller compared to samples based on the L13 (353 111 PFs). Most importantly, results show that diurnal cycles would remain similar if the OMI index data were used, although the OMI-based diurnal cycles show smaller variability between the suppressed and active phases (not shown). Therefore, the real-time L13 index may better represent the short-term variability in atmospheric conditions and is more relevant to diurnal variability than a time-filtered index. The real-time L13 index was able to adequately capture the influence of daily large-scale variability (Virts and Houze 2016; Xu and Rutledge 2018) and diurnal variations (Chudler et al. 2020) on convection.

3. Results

a. Diurnal cycles of rainfall, wind, and lightning

As expected, low-level atmospheric circulations and rainfall patterns over the key BSISO regions, including the SCS, the Philippines, and Indochina, change markedly between suppressed and active BSISO periods (Fig. 1). During suppressed BSISO periods (phases 1–3) over these areas, surface winds are relatively weak and precipitation is reduced. In contrast, active BSISO periods (phases 5–7) feature an enhanced rainband accompanied by strong low-level southwesterlies developing across these regions. However, rainfall in the ITCZ region (5°S to 5°N) where Borneo is located shows an off-phase pattern compared to the SCS; for example, Borneo has the most rainfall in phases 1–3 and the least in phases 5–7 [also see the phase-by-phase evolution in Xu and Rutledge (2018)]. In other words, precipitation over Borneo is enhanced during the SCS's suppressed BSISO periods but becomes suppressed during the SCS's active BSISO phases. A possible reason is that the active BSISO condition over the SCS may actually suppress convection over Borneo. After the BSISO onset over the SCS (phases 5–7), strong low-level convergence and convective scale ascent to the north of Borneo may cause compensating subsidence and drying over Borneo (Xu and Rutledge 2018).

Figure 2 shows the distribution of composited rainfall as well as surface wind anomalies at 1200–2300 LT (PM) versus 0000–1100 LT (AM) (3-hourly rainfall maps are shown in supplemental figures). During suppressed BSISO periods (phases 1–3; Figs. 2a–c), the SCS, the Philippines, and Indochina show peak afternoon convection over land and dominant nocturnal precipitation offshore due to land–sea breeze circulations (as shown by the onshore and offshore wind anomalies), consistent

JOBNAME: JCLI 00#00 2021 PAGE: 7 SESS: 8 OUTPUT: Tue Apr 6 06:10:19 2021 Total No. of Pages: 18
/ams/jcli/0/jcliD200308

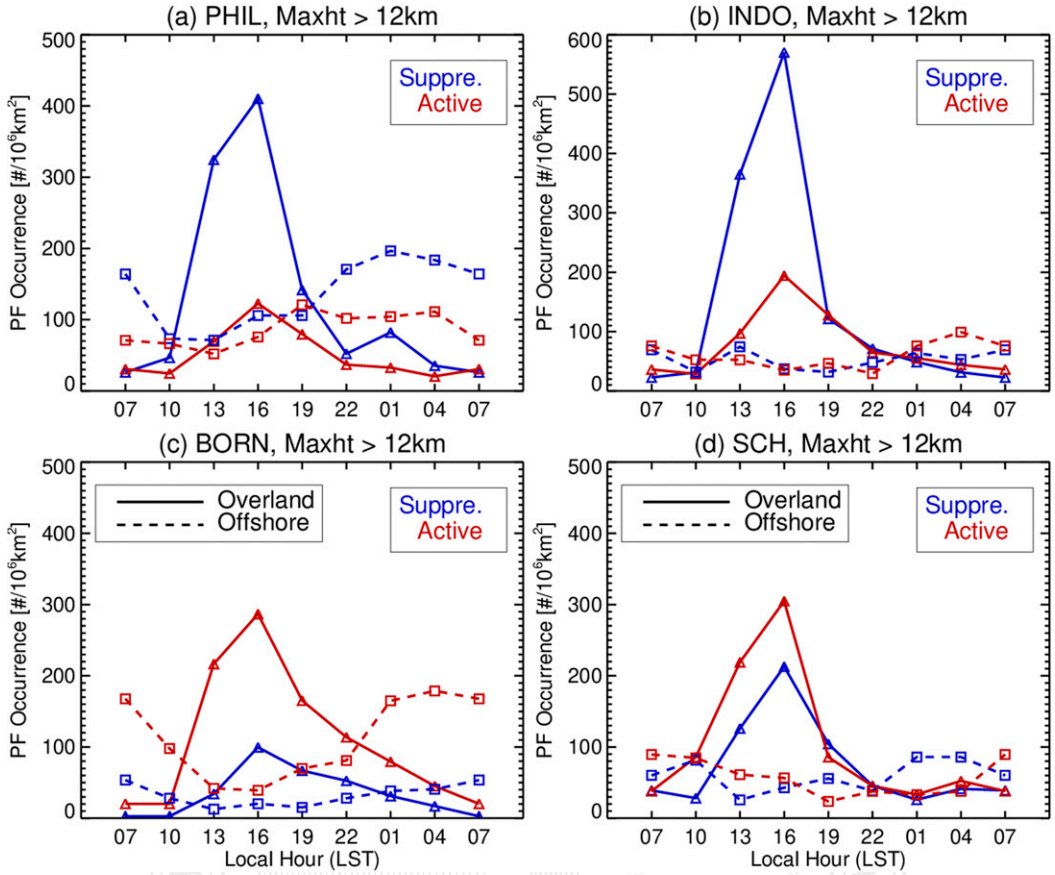

FIG. 5. Diurnal cycles of populations of deep convective features (height of 20 dBZ > 12 km) for overland (solid) and offshore (dashed) areas of selected regions during their suppressed (blue) and active (red) BSISO periods. PF population is normalized by the area of specific study regions; therefore, the y axis stands for the number of PFs within an area of 10^6 km^2.

with previous studies (Takahashi et al. 2010; Houze et al. 1981; Ichikawa and Yasunari 2006; Kanamori et al. 2013). Borneo shows the strongest offshore morning precipitation signal during its active BSISO periods (phases 1–3), with marked precipitation (accompanied by significant offshore wind anomalies) extending 200–300 km off the west coast. Nocturnal offshore precipitation is also obvious over the Philippines during suppressed BSISO periods (Fig. 2a), except over northern Luzon where maximum offshore precipitation occurs in the afternoon/evening (Fig. 2a). Closer examination shows that afternoon convection initiated over northern Luzon already starts to move offshore at 1900 LT and dissipates at 2200 LT (Fig. S2). In contrast, offshore precipitation in the central and southern Philippines mainly develops in the early morning (0100–0400 LT) due to land-breeze effects (Fig. S2).

After the onset of the BSISO over the SCS, the Philippines, and Indochina, land-based convection in these regions still shows a pronounced PM peak, and AM offshore precipitation remains significant in most of the coastal areas (Figs. 2d–f). The exception is western Philippines, where offshore precipitation persists through the day associated with the active BSISO rainband, although the overall rainband weakens somewhat in the evening (Fig. S3). However, overland convection in this region still exhibits a strong diurnal cycle with intense precipitation developing in early afternoon (1300 LT) and dissipating in late evening (2200 LT; Fig. S3). Overland intense convection in Indochina persists through 0400 LT (Fig. S3), possibly due to nocturnal orographic enhancement induced by katabatic winds from mountain ranges (Ruppert et al. 2013). The areal extension and amplitude of nocturnal rainfall off the western Borneo coast reduce significantly during its suppressed BSISO periods (phases 5–7) compared to active BSISO periods (phases 1–3). Two southwest–northeast-oriented bands of PM rainfall anomalies appear over the waters of northern and southern SCS, each 400–500 km away from the coast (Fig. 2f). Aves and Johnson (2008) showed that precipitation initiated off the southern China coast could propagate offshore as far as 500 km.

In terms of lightning, flash density displays a strong afternoon/evening maximum over land regardless of BSISO phase, even though lightning is much less frequent during active BSISO phases, especially over the Philippines and Indochina (Fig. 3). F3 Flash densities over Borneo are similar between suppressed and active BSISO phases, but their geographic distributions show very different patterns (Figs. 3a,c). For example, maximum PM

JOBNAME: JCLI 00#00 2021 PAGE: 8 SESS: 8 OUTPUT: Tue Apr 6 06:10:20 2021 Total No. of Pages: 18
/ams/jcli/0/jcliD200308

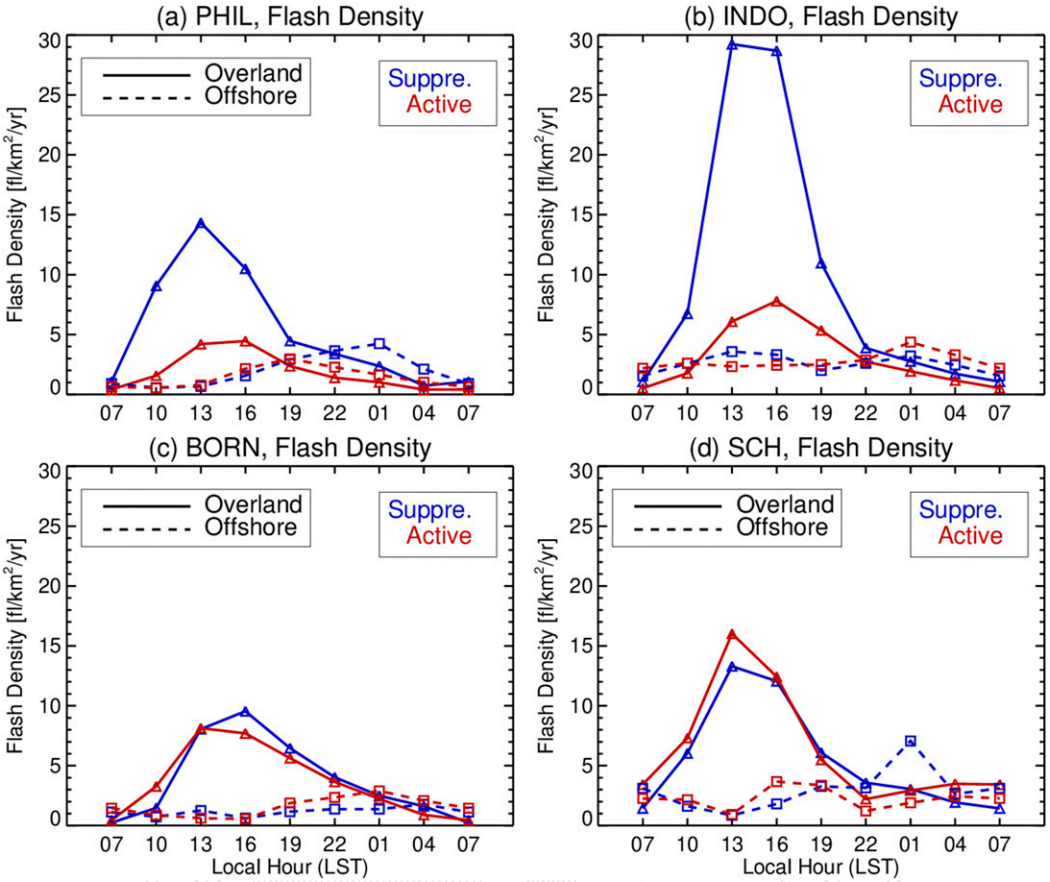

FIG. 6. As in Fig. 5, but for lightning flash density.

lightning is located mainly along the coasts during Borneo's active BSISO periods (phases 1–3) but concentrates more over the mountainous areas during suppressed BSISO periods (phases 5–7). The remarkable AM rainfall maximum offshore of the western Philippines (Fig. 2b) and Borneo (Fig. 2e) produces only marginal lightning, indicating the convection is weak to moderate in intensity (Fig. 3d). Offshore lightning is most frequent in the western Philippines during suppressed BSISO periods (Fig. 3b) when offshore rainfall is markedly reduced compared to active BSISO phases (Fig. 1). A southwest–northeast-oriented band of enhanced lightning appears over the southern/central SCS during active BSISO periods (Fig. 3d). This lightning band resembles the enhanced lightning zone over shipping lanes due to convective invigoration by aerosols emitted from passing ship traffic (Thornton et al. 2017). However, it is intriguing as to why lightning enhancement over SCS is most evident in the morning during active BSISO period compared to afternoon/evening, given that mean precipitation rates are similar between AM and PM hours (Figs. 2d,e).

b. Diurnal variations on convective characteristics

Diurnal cycle time series (3 hourly) of rain rates (by precipitation type) and convective characteristics are discussed in this section. Convective variables include deep convective occurrence, lightning flash density, frequency of organized MCS, and rainfall contribution by PF size. Four regions have been selected for these analyses including the Philippines, Indochina, Borneo, and southern China (marked in Fig. 1c). Each region is further separated into land and offshore areas to study the land-based and offshore convection, respectively.

Figure 4 demonstrates the time series of areal mean rain rate (separated into convective and stratiform rain types) over various regions (both land and offshore) during their suppressed and active BSISO periods. The phase and magnitude of diurnal variations on total rainfall as well as convective/stratiform precipitation type vary regionally and intraseasonally. Over the key BSISO regions (i.e., the Philippines and Indochina), active BSISO delays or extends both the land-afternoon and offshore-morning rainfall peaks (Figs. 4a,b), largely due to the increase of stratiform precipitation (red solid bars). For instance, convective precipitation peaks are similar between suppressed and active BSISO over the Philippines/Indochina, but stratiform rain maxima during active BSISO periods are double the amounts during suppressed BSISO periods. Enhanced stratiform precipitation also tends to be more persistent over larger landmasses (e.g., Indochina and Borneo) compared to relatively smaller islands (the Philippines). Of course, convective precipitation also increases from suppressed to active BSISO periods

JOBNAME: JCLI 00#00 2021 PAGE: 9 SESS: 8 OUTPUT: Tue Apr 6 06:10:20 2021 Total No. of Pages: 18
/ams/jcli/0/jcliD200308

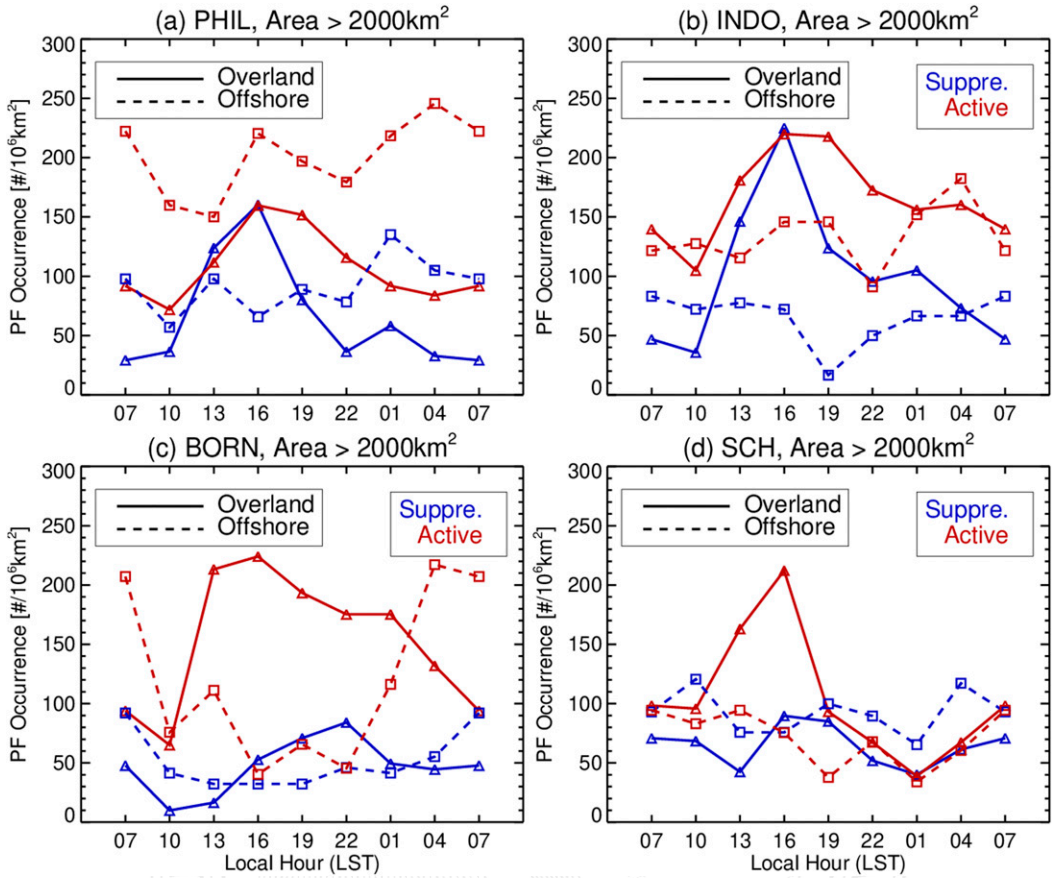

FIG. 7. As in Fig. 5, but for MCSs (PFs with area > 2000 km^2).

due to the increase of convective occurrence. Over Borneo, both the phase and amplitude of diurnal cycle of overland precipitation change substantially between suppressed and active BSISO periods. During active BSISO periods, total precipitation (convective precipitation as well) maximizes at 1600 LT and is extended through the evening (until 0100 LT) due to the increase of stratiform precipitation. During suppressed BSISO periods, convective precipitation over Borneo surprisingly peaks in the late evening (2200 LT) and is in phase with stratiform precipitation. Offshore precipitation around Borneo during active BSISO periods is twice that of the suppressed BSISO, and the increase is mainly contributed by morning precipitation (both convective and stratiform). In contrast, Southern China displays only subtle intraseasonal variability on rainfall diurnal cycle, consistent to its smaller convective variability on the intraseasonal scale (Xu and Rutledge 2018).

Diurnal cycles of deep convective features (height of 20 dBZ > 12 km) and lightning flash density are shown in Figs. 5 and 6. For comparison purposes, the deep convective populations are normalized by areas of the specific study regions. Deep convective features strongly peak at late afternoon over land, while over offshore/coastal areas deep convection maximizes in the morning with much smaller amplitudes (Fig. 5). Over Borneo, deep convective features increase from suppressed to active BSISO periods, and their diurnal variability becomes stronger during active periods. Interestingly, both the population and diurnal cycle amplitude of deep convective cells over the Philippines and Indochina reduce substantially during active BSISO periods, especially over land. Relatively few deep convective features (or cores) over land survive through the evening even during active BSISO periods when large-scale conditions are supportive for general convection. Lightning reveals similar diurnal cycles as deep convective features (Fig. 6), except that lightning density (or frequency) peaks 3 h earlier. It is possible mixed-phase ice process develop first, promoting storm electrification (Takahashi 1978), and then convective cells glaciate allowing small ice particles to be lofted to greater heights. The onset timing of maximum lightning density is also delayed 3 h after the BSISO onset over the Philippines and Indochina, even though deep convection peaks at the same time regardless of BSISO periods. In contrast, the diurnal cycle of lightning shows little intraseasonal variability over Borneo and southern China.

Figure 7 shows the diurnal cycles of organized convection (MCS) as defined by PF area > 2000 km^2, following the definition used by Xu and Rutledge (2018) and other TRMM studies (Nesbitt et al. 2000). Generally, MCSs show similar diurnal variations as total precipitation (Fig. 4) but differ from

JOBNAME: JCLI 00#00 2021 PAGE: 10 SESS: 8 OUTPUT: Tue Apr 6 06:10:21 2021 Total No. of Pages: 18
/ams/jcli/0/jcliD200308

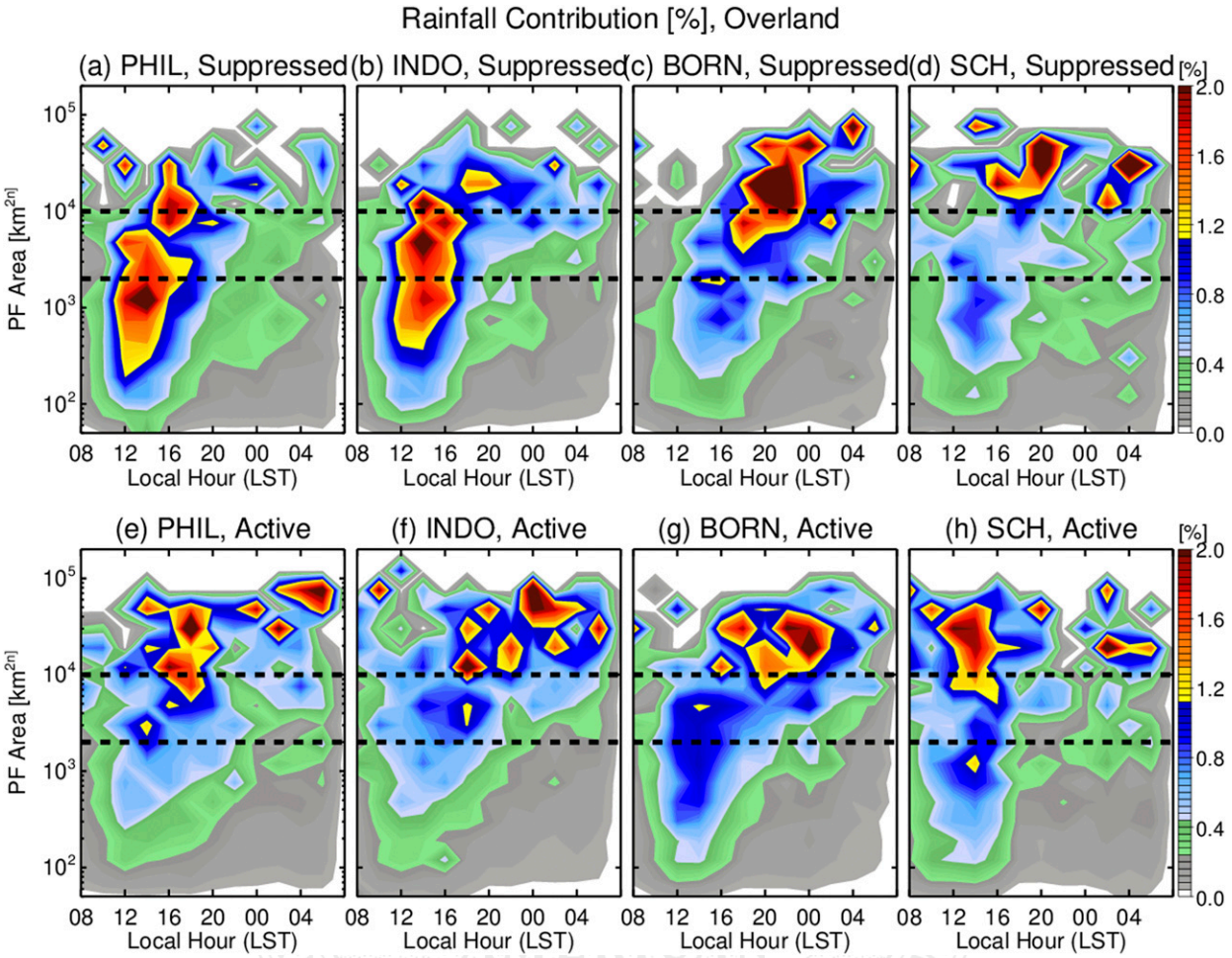

FIG. 8. Rainfall contribution (%) as a function of PF size (*y* axis) and local time of the day (*x* axis) for overland areas of selected regions during their (a)–(d) suppressed and (e)–(h) active BSISO periods.

deep convective features to some degree (Fig. 5). During suppressed BSISO, overland MCS populations peak at the same time (1600 LT) as deep convective features over Philippines and Indochina (Figs. 7a,b), suggesting only limited upscale growth under the suppressed BSISO conditions (e.g., drier conditions, lower wind shear, and large-scale descending motion). In contrast, overland MCSs are much extended in time during active BSISO periods due to upscale growth, consistent with the trend in stratiform precipitation (Fig. 4). Over the Philippines and Indochina, although deep convective features occur more frequently during suppressed BSISO than active BSISO (Figs. 5a,b) periods, peak MCS populations are similar in these two periods (Figs. 6a,b). This again indicates that during suppressed BSISO periods a large number of deep convective cells over these regions do not go through upscale growth or organize into MCS structures. Over Borneo, the MCS population over the island maximizes at 1600 LT and a great portion of MCS activity is maintained through the evening (0100 LT) during active BSISO periods. Offshore MCSs show only limited diurnal variability for most regions, except over Borneo, where a remarkable number of MCSs develop offshore at 0400–0700 LT.

Rainfall contribution as a function of precipitation system size (PF rain area) and time (local hour) are depicted in Figs. 8 and 9. Rainfall contribution is defined as the total volumetric rain (area multiplied by rain rate) of PFs in a specific time (2 h) and PF area bin to the total volumetric rain from all PFs. Over the Philippines and Indochina, a major fraction (>70%) of rainfall during suppressed BSISO phases is contributed by small to medium systems (e.g., $<10\,000\ km^2$) in the afternoon (1200–1800 LT). In particular, afternoon isolated convection or non-MCSs precipitation ($<2000\ km^2$) contributes 40% of the rainfall. In contrast, nighttime (after 1800 LT) broad precipitation systems (e.g., $>10\,000\ km^2$) are responsible for more than 70% of the active BSISO rainfall. Also, the growth rate of precipitation systems (defined by the slope of frequency contours relative to time) during suppressed BSISO periods is much higher than during active BSISO periods. During suppressed BSISO periods, a nontrivial portion (20%) of rainfall over Indochina is attributed

JOBNAME: JCLI 00#00 2021 PAGE: 11 SESS: 8 OUTPUT: Tue Apr 6 06:10:21 2021 Total No. of Pages: 18
/ams/jcli/0/jcliD200308

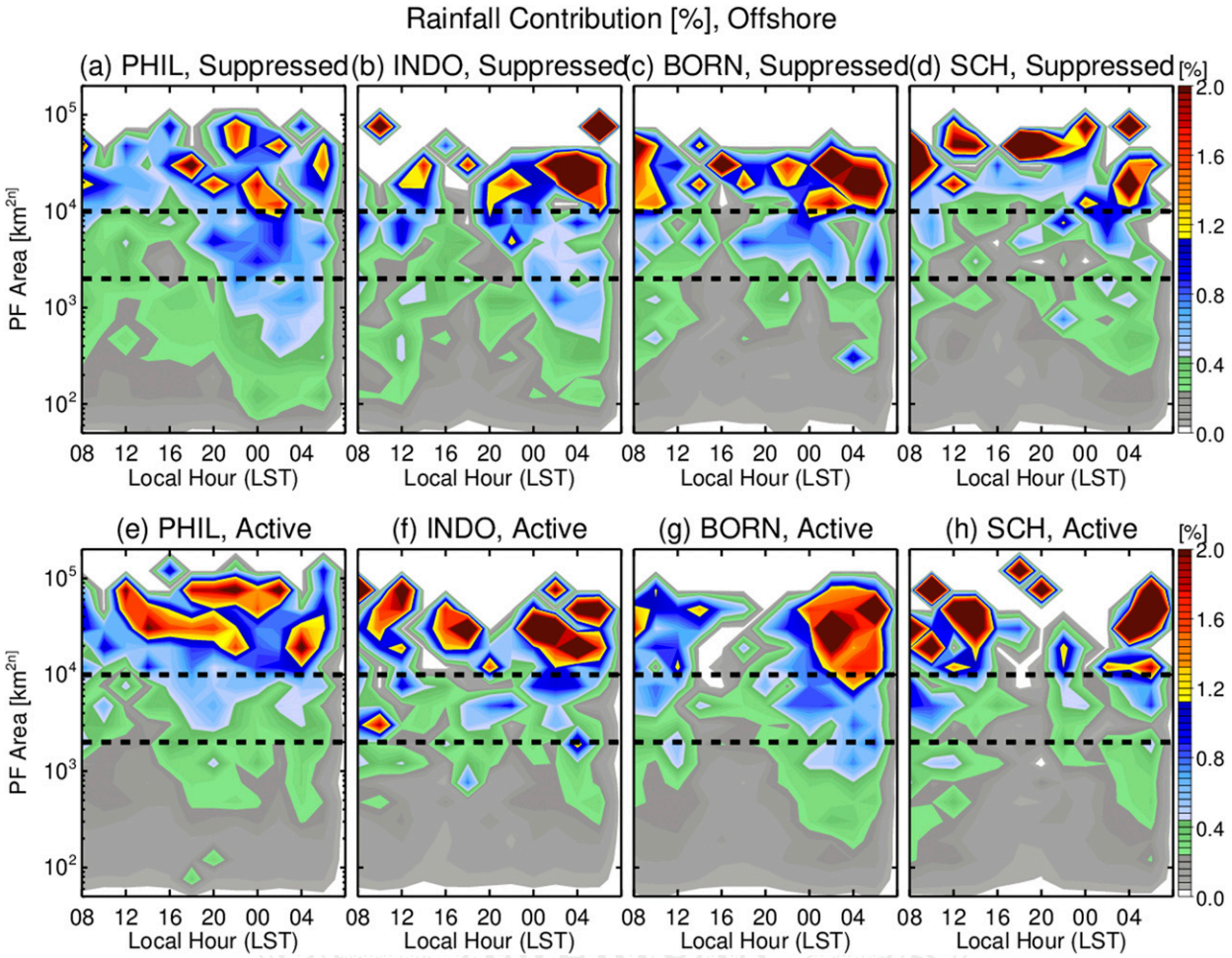

FIG. 9. As in Fig. 8, but for offshore areas.

to large, nocturnal PFs (>10 000 km^2) possibly due to nocturnal precipitation enhancement over inland valleys or mountain foothills (Fig. 2). Over Borneo, both suppressed and active BSISO periods have a major portion (>70%) of total precipitation contributed by very large PFs occurring after 1800 LT. Active BSISO periods exhibit a greater fraction of rainfall due to isolated convection over Borneo than during suppressed BSISO periods, even though MCSs are more frequent in active BSISO phases of this region (Fig. 7c). Over Southern China, most of the rainfall (>80%) during active BSISO periods occurs between 1200 and 1600 LT through contributions from both small and large systems. It is interesting that during active BSISO periods many extremely large PFs (>10 000 km^2) develop in the early afternoon (1200–1500 LT) and contribute more than half of the total precipitation in Southern China. As far as offshore precipitation, it is mainly contributed by large PFs (>10 000 km^2) for all the regions (Fig. 11). Isolated convective features or non-MCS systems (<2000 m^2) induce only a small rainfall fraction (<10%) regardless of BSISO phases. This suggests that offshore precipitation is mostly due to 1) enhancement of the offshore propagation of land-based convection instead of locally developed convective systems (Houze et al. 1981) or 2) long-duration large MCSs developing offshore fed by upstream convective systems (Xu et al. 2012).

c. *Precipitation propagation and vertical cross sections*

This section discusses the diurnal variations on potential propagation and vertical structure of convection over selected regions crossing the western coasts of Luzon and Borneo, where offshore precipitation is most enhanced (marked in Fig. 1d). The occurrence frequency or "cross section" of 20-dBZ radar reflectivity as a function of height and horizontal distance (from the coast) is derived from 17-yr combined vertical radar profiles of PR within the cross-section band (Figs. 10–13). F10 F13

Figure 10 demonstrates that during suppressed BSISO periods, convection initiates over Luzon Island around noon (1100–1300 LT), vertically develops into deep convection (>12 km) during late afternoon (1400–1700 LT) and grows upscale in the evening (1800–2000 LT). Precipitation starts to

JOBNAME: JCLI 00#00 2021 PAGE: 12 SESS: 8 OUTPUT: Tue Apr 6 06:10:22 2021 Total No. of Pages: 18
/ams/jcli/0/jcliD200308

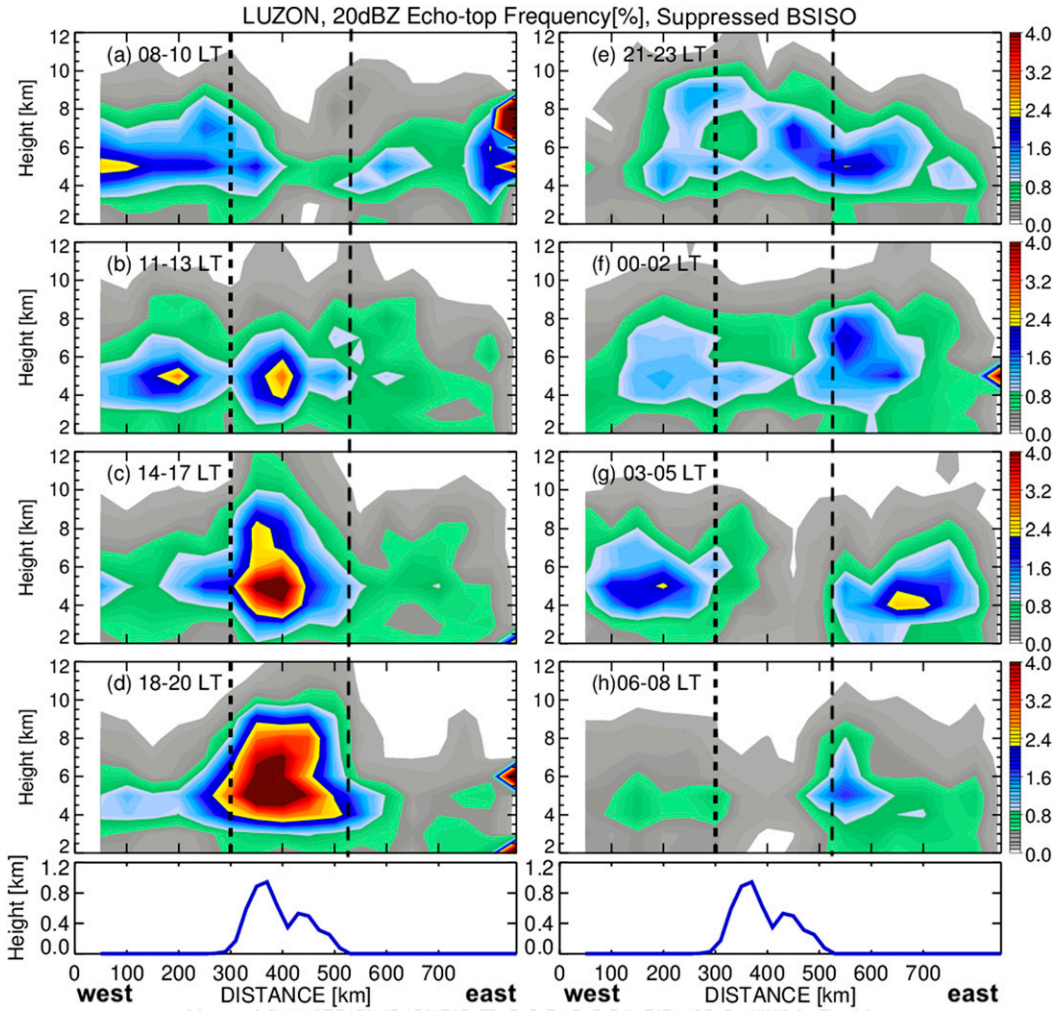

FIG. 10. (a)–(h) Occurrence frequency of 20-dBZ radar reflectivity for a cross section over Luzon as a function of distance (in km) from the western coast (x axis) and altitude (y axis) for every 3 h of the day during suppressed BSISO periods. Dashed lines approximately mark the coastal lines. (bottom) Elevations averaged along the cross section.

develop offshore (off both west and east coasts) and propagates away during late evening (2100–2300 LT) when overland convection dissipates after midnight (0000–0200 LT). Since offshore convection (off the west coast) that develops in the 0000–0200 LT period dissipates by the midmorning (0600–0800 LT), significant offshore convection reappearing in the late morning (0800–1100 LT) is possibly due to precipitation systems propagating from the upstream ocean (to the southwest) as indicated by 3-h rainfall maps (Fig. S1). The active BSISO shows a very different precipitation "vertical cross section" (Fig. 11). During the active BSISO, offshore deep convection generally persists through the day, while overland deep convection exhibits a strong diurnal cycle, which peaks at 1800–2000 LT. Specifically, the widespread offshore convection is enhanced in the morning (0300–1000 LT; 20-dBZ echo tops higher than 10 km), but convection becomes relatively shallower (20-dBZ echo-top height < 7 km) in the afternoon and evening (1400–2300 LT). Offshore deep convection does not extend into land areas until the afternoon (1200–1400 LT) when the overland condition is favorable for convection once again. Overland convection develops vertically and upscale through the afternoon and achieves its greatest depth at 1800–2000 LT (20-dBZ echo tops higher than 10 km). Overland precipitation depth (or convective intensity) substantially decreases near midnight (0000–0200 LT). Significant frequency of lower-depth precipitation (lower than 5–6 km), indicative of major stratiform precipitation, persists for a longer time through the midmorning (0800–1000 LT).

Over Borneo, precipitation of shallow to medium depth dominates in the morning during active BSISO periods (Fig. 12), possibly contributed by shallow rain showers or stratiform precipitation over mountain valleys or foothills induced by nocturnal mountain-valley circulations. In the same BSISO periods, convective depth over land substantially increases at

JOBNAME: JCLI 00#00 2021 PAGE: 13 SESS: 8 OUTPUT: Tue Apr 6 06:10:22 2021 Total No. of Pages: 18
/ams/jcli/0/jcliD200308

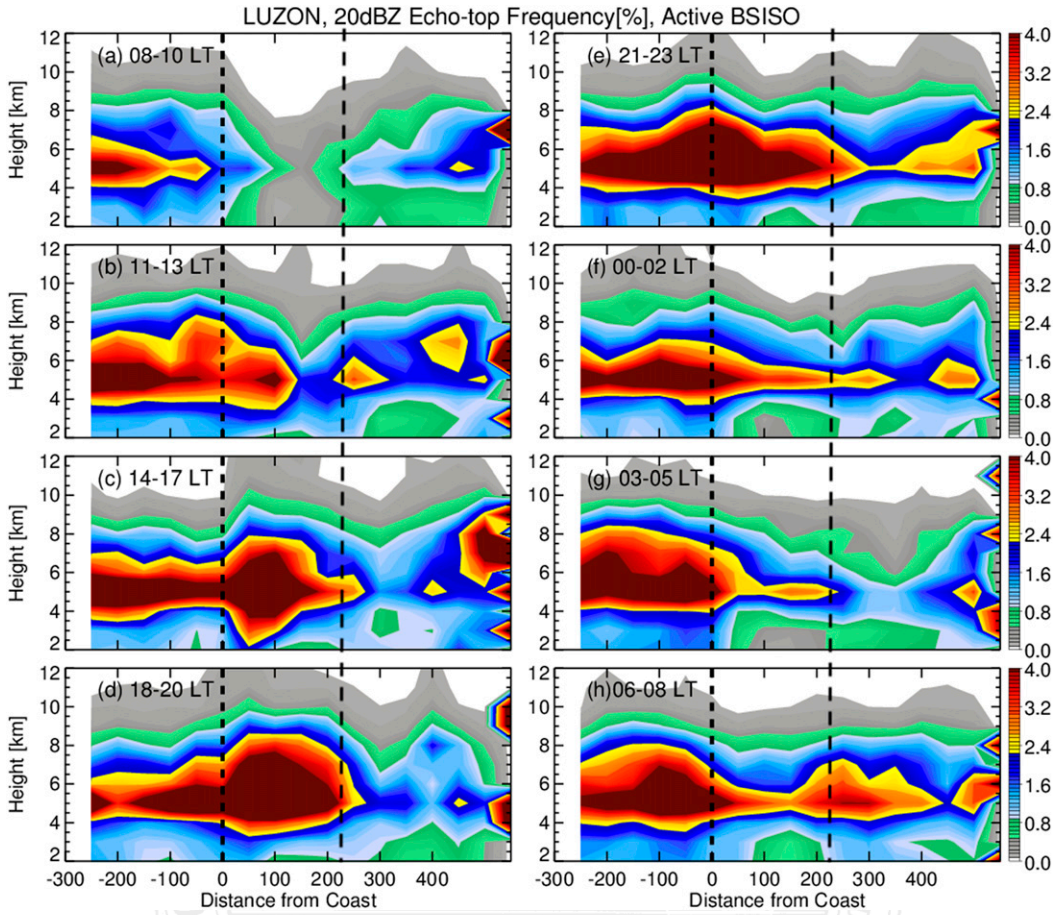

FIG. 11. As in Fig. 10, but for active BSISO periods.

1400–1700 LT and maximizes in the late evening (2100–2300 LT; e.g., 20-dBZ echo tops reaching above 11 km). Deep convection starts to propagate offshore along the west coast at 0000–0200 LT, and reintensifies just offshore at 0300–0500 LT. The deep convective center is located 200 km off the coast at 0800–1000 LT. During suppressed BSISO periods, convection over Borneo is generally reduced (with much lower precipitation occurrence) and shows a distinctly different "vertical radar cross section" compared to active BSISO phases (Fig. 13). Only limited shallow to moderate convection develops over land throughout the afternoon, and deep convective frequency maximizes in the late evening (2100–2300 LT) over the mountains. Deep overland convection dissipates very quickly in the morning. Offshore precipitation initiates around 0300–0500 LT and propagates seaward through the morning, reaching its greatest depth 200 km offshore by 0800–1000 LT.

4. Summary and discussion

This study investigates how the diurnal cycle of convection in the SCS region is modulated by the BSISO (i.e., variability of the diurnal cycle between suppressed and active BSISO periods). While this has been the similar subject of earlier studies (as reviewed in the introduction), the current study extends our knowledge on the rainfall diurnal cycle to diurnal variations of convective characteristics such as precipitation type, deep convective feature, lightning, MCS, and precipitation vertical structure. In addition to surface rainfall and winds, diurnal cycles of convective characteristics over various coastal areas (both overland and offshore) have been studied in detail using longer-term three-dimensional radar measurements and rain-rate estimates from spaceborne precipitation radar. Figure 14 F14 summarizes how the suppressed and active BSISO modulates the diurnal cycle of convection over Philippines/Indochina and western Borneo, where the prevailing low-level flows are perpendicular and parallel to coast lines, respectively.

Over the Philippines and Indochina, the diurnal cycle of convection is substantially enhanced during suppressed BSISO periods and delayed during active periods, consistent with changes of diurnal cycle over the MC due to the MJO (Sui and Lau 1992; Rauniyar and Walsh 2011; Sakaeda et al. 2017). During suppressed periods, intense surface heating (due to stronger solar insolation under cloud-free conditions) promotes large CAPE values, which enables strong land-based afternoon convection and heavy rainfall. Afternoon deep convection and lightning are the most prevalent at this time. In

JOBNAME: JCLI 00#00 2021 PAGE: 14 SESS: 8 OUTPUT: Tue Apr 6 06:10:22 2021 Total No. of Pages: 18
/ams/jcli/0/jcliD200308

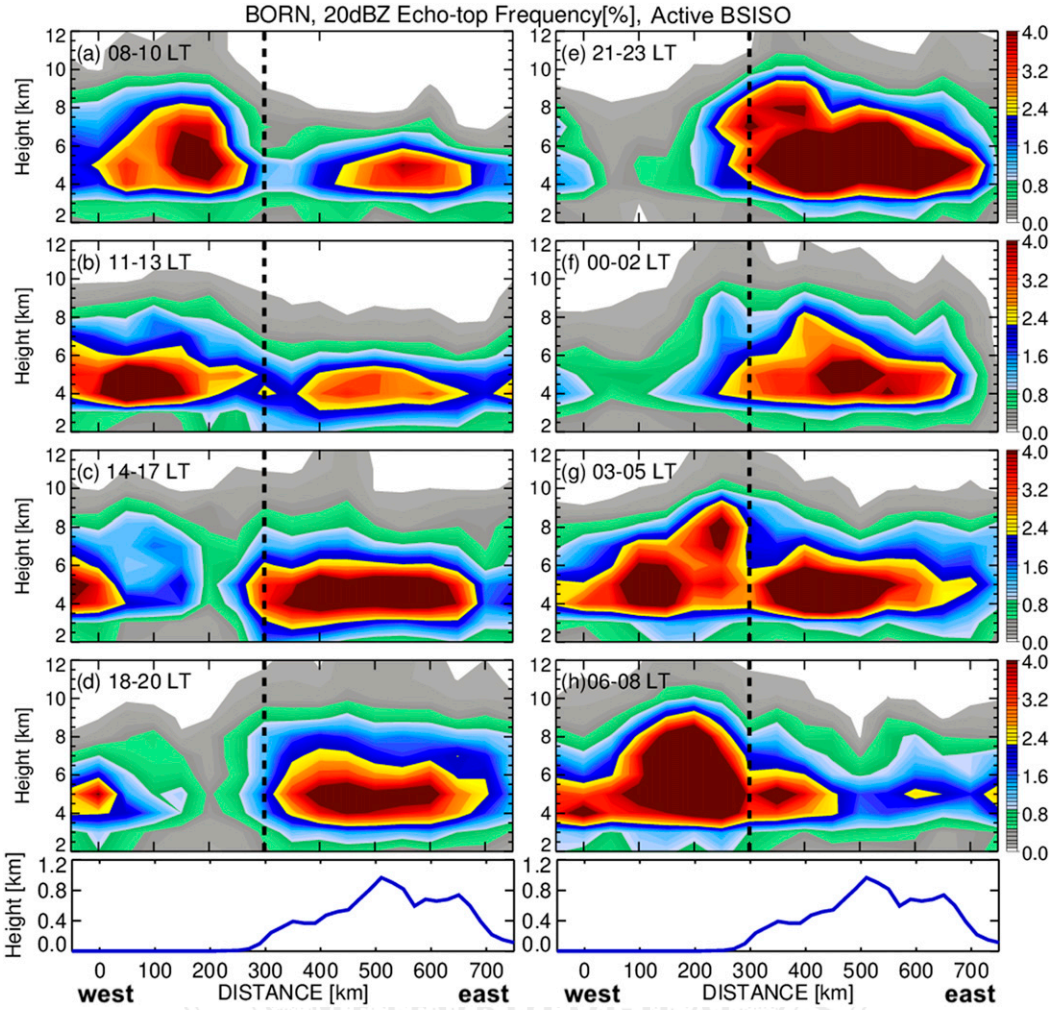

AU2 FIG. 12. As in Fig. 10, but for Borneo region during active BSISO periods.

addition, the diurnal cycle of convection offshore of the western Philippines is stronger and exhibits a significant propagation signal during these periods. This is possibly because the warmer SST (high surface air temperature over the water) and stronger nighttime radiative cooling (due to reduced cloudiness) during suppressed periods may induce land–sea breeze circulations whose magnitudes are comparable to the prevailing low-level onshore flows. As a result, offshore convection varies diurnally. During active BSISO periods, the diurnal cycle is still evident over the Philippines, and rainfall peaks are extended/delayed. Specifically, the moist and high shear environments of active periods promote overland MCS development through the enhancement of stratiform precipitation, therefore significantly extending the afternoon rainfall peak. However, diurnal cycles of intense convection and lightning activity over the Philippines during active periods are markedly reduced due to lower CAPE (caused by persistent cloudy conditions reducing surface heating). On the other hand, the diurnal cycle of offshore precipitation over the Philippines is fairly weak and heavy rainfall persists through the day during active BSISO phases, as the strong prevailing low-level flows impinge on coastal terrains causing significant lifting or converge with the relatively weak onshore–offshore flows along the coasts.

Over Borneo, diurnal cycles (both onshore and offshore) are stronger during active BSISO periods than suppressed periods, contrasting to the situation over Philippines/Indochina. During suppressed BSISO periods, large-scale environments over Borneo are less favorable for convective development, possibly due to drier low-levels and upper-level subsidence caused by persistent deep convection to the north (over SCS). These conditions actually suppress the coastal convection in the afternoon, and therefore peak convection is limited to the island's highest terrain until the convective suppression is overcome in the late afternoon or evening. In contrast, the moist and ITCZ-like conditions during active BSISO periods are supportive of convective development (e.g., marked afternoon peak convection over land and nocturnal maximum precipitation offshore). Also, the large landmass and mountainous terrain (e.g., stronger and uneven surface heating) of

JOBNAME: JCLI 00#00 2021 PAGE: 15 SESS: 8 OUTPUT: Tue Apr 6 06:10:23 2021 Total No. of Pages: 18
/ams/jcli/0/jcliD200308

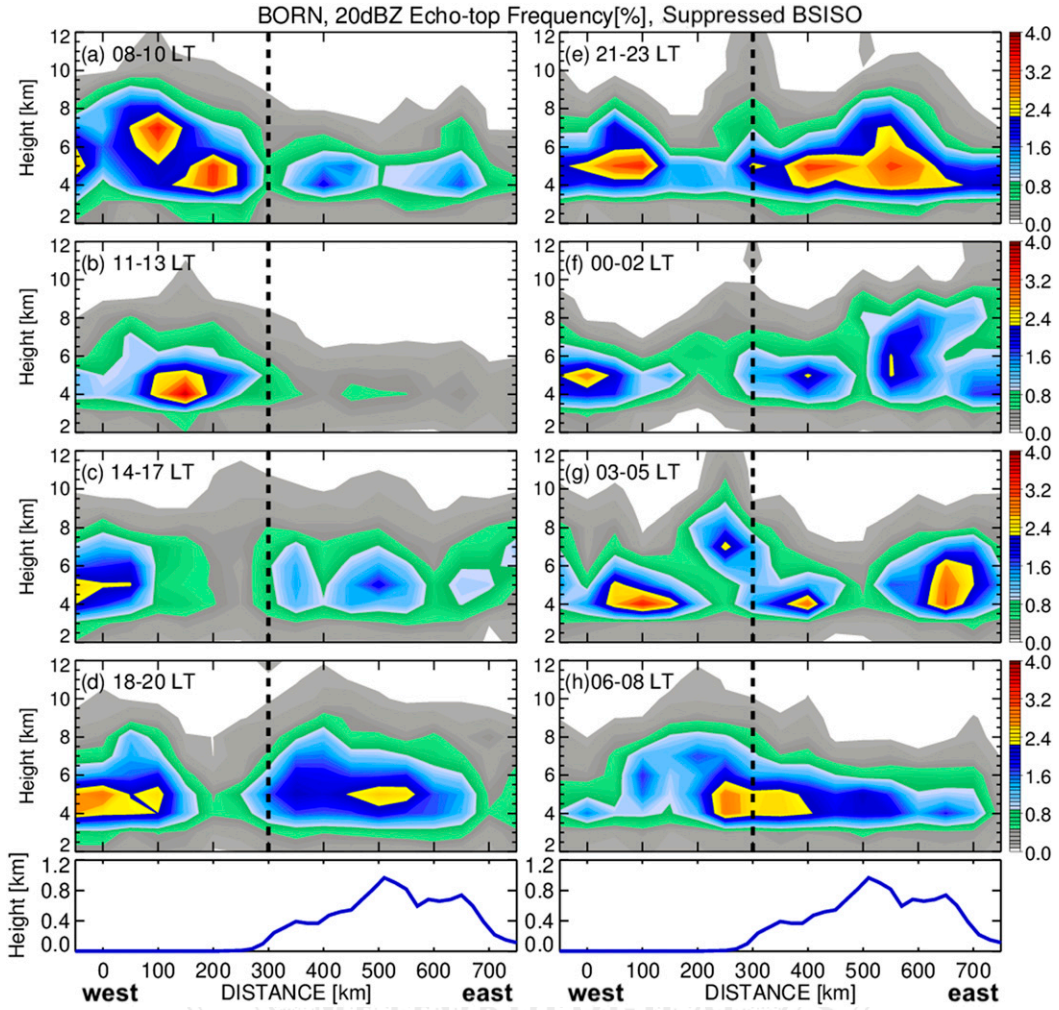

FIG. 13. As in Fig. 10, but for Borneo region during suppressed BSISO periods.

Borneo may further enhance the afternoon overland convection. MCSs are much longer-lived during active periods possibly due to a moister environment, although diurnal cycles of deep convective features and lightning are invariant.

Compared to the Philippines, western Borneo shows much greater diurnal variations on offshore convection during active periods, featured by a strong nocturnal peak and marked offshore propagation. This is similar to the case that diurnal convective disturbances over the MC propagate farther offshore during active MJO phases (Rauniyar and Walsh 2011; Sakaeda et al. 2017). A potential explanation here is that the land–sea breeze over western Borneo is perpendicular to the prevailing monsoon flow, therefore, diurnal cycle of offshore convection is strongly tied to the land–sea breezes. During suppressed (active) BSISO periods in Borneo, the prevailing low-level winds over the SCS are enhanced (reduced), which cool (warm) the SST through increasing (decreasing) upper-ocean mixing. As a result, the warmer SST (high surface air temperature over the water) during active periods may induce a stronger nighttime land breeze over western Borneo (warm ocean, cool land at night). Of course, active periods over Borneo provides a more favorable environment for convective development and offshore propagation when the land breeze converges with the prevailing low-level winds over the ocean.

Acknowledgments. This research was supported by the U.S. Office of Naval Research PISTON program (Grant N000141613092), the National Natural Science Foundation of China (Grant 41975053),and the Guangdong Provincial Department of Science and Technology, China (Grants 2019QN01G107 and 2019ZT08G090). All three anonymous reviewers are much appreciated for their constructive comments and suggestions in improving this paper. We thank Professors Edward Zipser (University of Utah) and Chuntao Liu (TAMU-CC) for providing the TRMM precipitation feature dataset. Thanks also go to Prof. June-Yi Lee for providing the BSISO index data. The TRMM precipitation features and orbital lightning data can be downloaded from

JOBNAME: JCLI 00#00 2021 PAGE: 16 SESS: 8 OUTPUT: Tue Apr 6 06:10:23 2021 Total No. of Pages: 18
/ams/jcli/0/jcliD200308

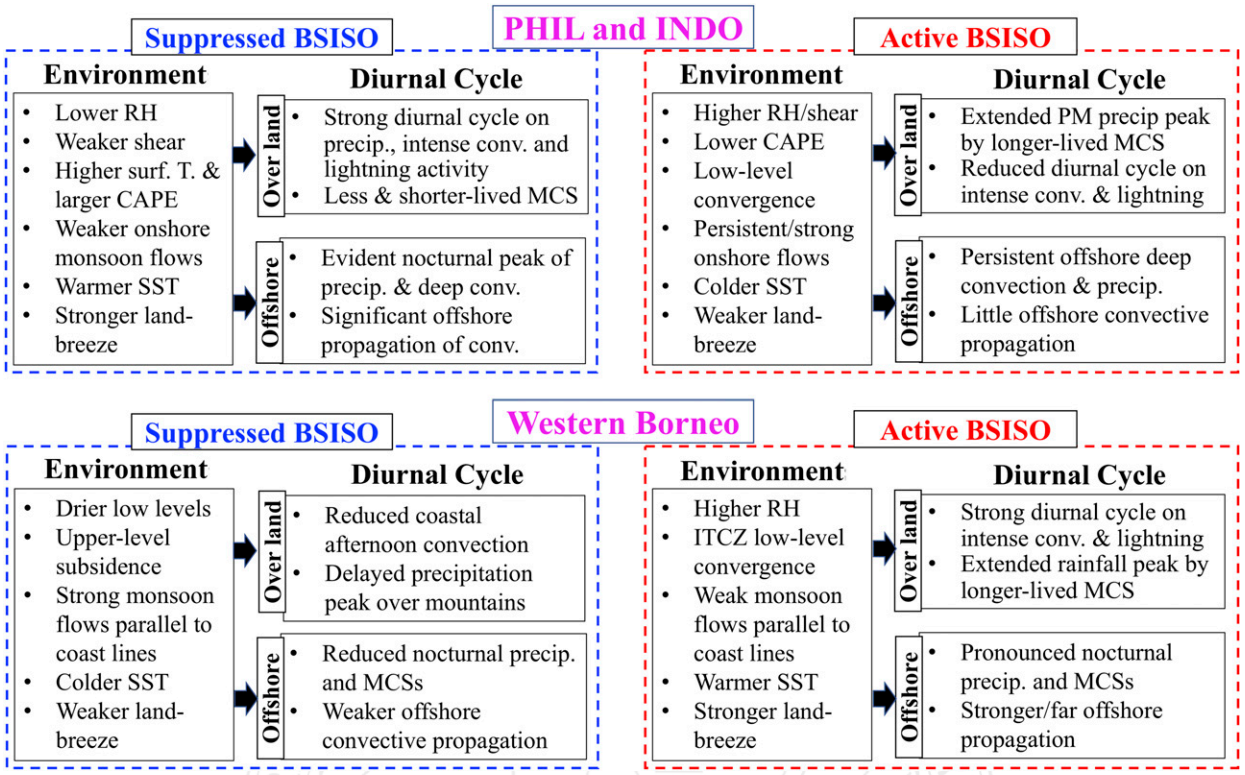

FIG. 14. Schematic summary on changes of large-scale environments and variations on diurnal cycles over (top) the Philippines and (bottom) western Borneo between suppressed and active BSISO periods. Diurnal cycle characteristics are separately summarized for over land and offshore.

NASA Goddard Earth Sciences Data and Information Services Center (http://disc.sci.gsfc.nasa.gov/TRMM), CCMP wind estimates are available at http://www.remss.com/measurements/ccmp/, and BSISO index data from http://iprc.soest.hawaii.edu/users/jylee/bsiso.

REFERENCES

Atlas, R., R. N. Hoffman, J. Ardizzone, S. M. Leidner, J. C. Jusem, D. K. Smith, and D. Gombos, 2011: A cross-calibrated, multiplatform ocean surface wind velocity product for meteorological and oceanographic applications. *Bull. Amer. Meteor. Soc.*, **92**, 157–174, https://doi.org/10.1175/2010BAMS2946.1.

Aves, S. L., and R. H. Johnson, 2008: The diurnal cycle of convection over the northern South China Sea. *J. Meteor. Soc. Japan*, **86**, 919–934, https://doi.org/10.2151/jmsj.86.919.

Birch, C. E., S. Webster, S. C. Peatman, D. J. Parker, A. J. Matthews, Y. Li, and M. E. E. Hassim, 2016: Scale interactions between the MJO and the western Maritime Continent. *J. Climate*, **29**, 2471–2492, https://doi.org/10.1175/JCLI-D-15-0557.1.

Boccippio, D. J., W. J. Koshak, and R. J. Blakeslee, 2002: Performance assessment of the Optical Transient Detector and Lightning Imaging Sensor. Part I: Predicted diurnal variability. *J. Atmos. Oceanic Technol.*, **19**, 1318–1332, https://doi.org/10.1175/1520-0426(2002)019<1318:PAOTOT>2.0.CO;2.

Chen, X., F. Zhang, and J. H. Ruppert, 2019: Modulations of the diurnal cycle of coastal rainfall over South China caused by the boreal summer intraseasonal oscillation. *J. Climate*, **32**, 2089–2108, https://doi.org/10.1175/JCLI-D-18-0786.1.

Christian, H. J., 1999: Optical detection of lightning from space. *Proc. 11th Int. Conf. on Atmospheric Electricity*, Guntersville, AL, ICAE, 715–718.

——, and Coauthors, 2003: Global frequency and distribution of lightning as observed from space by the optical transient detector. *J. Geophys. Res.*, **108**, 4005, https://doi.org/10.1029/2002JD002347.

Chudler, K., W. Xu, and S. A. Rutledge, 2020: Impact of the boreal summer intraseasonal oscillation on the diurnal cycle of precipitation near and over the island of Luzon. *Mon. Wea. Rev.*, **148**, 1805–1827, https://doi.org/10.1175/MWR-D-19-0252.1.

DeMott, C. A., C. Stan, and D. A. Randall, 2013: Northward propagation mechanisms of the boreal summer intraseasonal oscillation in the ERA-Interim and SP-CCSM. *J. Climate*, **26**, 1973–1992, https://doi.org/10.1175/JCLI-D-12-00191.1.

Gopalan, K., N.-Y. Wang, R. Ferraro, and C. Liu, 2010: Status of the TRMM 2A12 land precipitation algorithm. *J. Atmos. Oceanic Technol.*, **27**, 1343–1354, https://doi.org/10.1175/2010JTECHA1454.1.

Ho, C.-H., M.-S. Park, Y.-S. Choi, and Y. N. Takayabu, 2008: Relationship between intraseasonal oscillation and diurnal variation of summer rainfall over the South China Sea. *Geophys. Res. Lett.*, **35**, L03701, https://doi.org/10.1029/2007GL031962.

Houze, R. A., Jr., S. G. Geotis, F. D. Marks Jr., and A. K. West, 1981: Winter monsoon convection in the vicinity of north Borneo. Part I: Structure and time variation of the clouds and precipitation. *Mon. Wea. Rev.*, **109**, 1595–1614, https://doi.org/10.1175/1520-0493(1981)109<1595:WMCITV>2.0.CO;2.

Ichikawa, H., and T. Yasunari, 2006: Time–space characteristics of diurnal rainfall over Borneo and surrounding oceans as observed by TRMM-PR. *J. Climate*, **19**, 1238–1260, https://doi.org/10.1175/JCLI3714.1.

——, and ——, 2007: Propagating diurnal disturbances embedded in the Madden–Julian Oscillation. *Geophys. Res. Lett.*, **34**, L18811, https://doi.org/10.1029/2007GL030480.

Iguchi, T., T. Kozu, R. Meneghini, J. Awaka, and K. Okamoto, 2000: Rain-profiling algorithm for the TRMM Precipitation Radar. *J. Appl. Meteor.*, **39**, 2038–2052, https://doi.org/10.1175/1520-0450(2001)040<2038:RPAFTT>2.0.CO;2.

Jiang, H., and E. Zipser, 2010: Contribution of tropical cyclones to the global precipitation from eight seasons of TRMM data: Regional, seasonal, and interannual variations. *J. Climate*, **23**, 1526–1543, https://doi.org/10.1175/2009JCLI3303.1.

Jiang, X., T. Li, and B. Wang, 2004: Structures and mechanisms of the northward propagating boreal summer intraseasonal oscillation. *J. Climate*, **17**, 1022–1039, https://doi.org/10.1175/1520-0442(2004)017<1022:SAMOTN>2.0.CO;2.

Kanamori, H., T. Yasunari, and K. Kuraji, 2013: Modulation of the diurnal cycle of rainfall associated with the MJO observed by a dense hourly rain gauge network at Sarawak, Borneo. *J. Climate*, **26**, 4858–4875, https://doi.org/10.1175/JCLI-D-12-00158.1.

Kemball-Cook, S., and B. Wang, 2001: Equatorial waves and air–sea interaction in the boreal summer intraseasonal oscillation. *J. Climate*, **14**, 2923–2942, https://doi.org/10.1175/1520-0442(2001)014<2923:EWAASI>2.0.CO;2.

Kiladis, G. N., J. Dias, K. H. Straub, M. C. Wheeler, S. N. Tulich, K. Kikuchi, K. M. Weickmann, and M. J. Ventrice, 2014: A comparison of OLR and circulation-based indices for tracking the MJO. *Mon. Wea. Rev.*, **142**, 1697–1715, https://doi.org/10.1175/MWR-D-13-00301.1.

Kikuchi, K., B. Wang, and Y. Kajikawa, 2012: Bimodal representation of the tropical intraseasonal oscillation. *Climate Dyn.*, **38**, 1989–2000, https://doi.org/10.1007/s00382-011-1159-1.

Knapp, K. R., M. C. Kruk, D. H. Levinson, H. J. Diamond, and C. J. Neumann, 2010: The International Best Track Archive for Climate Stewardship (IBTrACS): Unifying tropical cyclone best track data. *Bull. Amer. Meteor. Soc.*, **91**, 363–376, https://doi.org/10.1175/2009BAMS2755.1.

Kummerow, C., D. L. Randel, M. Kulie, N. Wang, R. Ferraro, S. Joseph Munchak, and V. Petkovic, 2015: The evolution of the Goddard profiling algorithm to a fully parametric scheme. *J. Atmos. Oceanic Technol.*, **32**, 2265–2280, https://doi.org/10.1175/JTECH-D-15-0039.1.

Lee, J. Y., B. Wang, M. C. Wheeler, X. Fu, D. E. Waliser, and I.-S. Kang, 2013: Real-time multivariate indices for the boreal summer intraseasonal oscillation over the Asian summer monsoon region. *Climate Dyn.*, **40**, 493–509, https://doi.org/10.1007/s00382-012-1544-4.

Liu, C., E. J. Zipser, D. J. Cecil, S. W. Nesbitt, and S. Sherwood, 2008: A cloud and precipitation feature database from nine years of TRMM observations. *J. Appl. Meteor. Climatol.*, **47**, 2712–2728, https://doi.org/10.1175/2008JAMC1890.1.

Mapes, B. E., T. T. Warner, and M. Xu, 2003: Diurnal patterns of rainfall in northwestern South America. Part III: Diurnal gravity waves and nocturnal convection offshore. *Mon. Wea. Rev.*, **131**, 830–844, https://doi.org/10.1175/1520-0493(2003)131<0830:DPORIN>2.0.CO;2.

Natoli, M. B., and E. D. Maloney, 2019: Intraseasonal variability of the diurnal cycle of precipitation in the Philippines. *J. Atmos. Sci.*, **76**, 3633–3654, https://doi.org/10.1175/JAS-D-19-0152.1.

Nesbitt, S. W., E. J. Zipser, and D. J. Cecil, 2000: A census of precipitation features in the tropics using TRMM: Radar, ice scattering, and lightning observations. *J. Climate*, **13**, 4087–4106, https://doi.org/10.1175/1520-0442(2000)013<4087:ACOPFI>2.0.CO;2.

Ogura, Y., and M. Yoshizaki, 1988: Numerical study of orographic-convective precipitation over the eastern Arabian Sea and the Ghat Mountains during the summer monsoon. *J. Atmos. Sci.*, **45**, 2097–2122, https://doi.org/10.1175/1520-0469(1988)045<2097:NSOOCP>2.0.CO;2.

Peatman, S. C., A. J. Matthews, and D. P. Stevens, 2014: Propagation of the Madden–Julian Oscillation through the Maritime Continent and scale interaction with the diurnal cycle of precipitation. *Quart. J. Roy. Meteor. Soc.*, **140**, 814–825, https://doi.org/10.1002/qj.2161.

Rauniyar, S. P., and K. J. E. Walsh, 2011: Scale interaction of the diurnal cycle of rainfall over the Maritime Continent and Australia: Influence of the MJO. *J. Climate*, **24**, 325–348, https://doi.org/10.1175/2010JCLI3673.1.

Ruppert, J. H., Jr., R. H. Johnson, and A. K. Rowe, 2013: Diurnal circulations and rainfall in Taiwan during SoWMEX/TiMREX (2008). *Mon. Wea. Rev.*, **141**, 3851–3872, https://doi.org/10.1175/MWR-D-12-00301.1.

Sakaeda, N., G. Kiladis, and J. Dias, 2017: The diurnal cycle of tropical cloudiness and rainfall associated with the Madden–Julian oscillation. *J. Atmos. Sci.*, **30**, 3999–4020, https://doi.org/10.1175/JCLI-D-16-0788.1.

Sui, C.-H., and K.-M. Lau, 1992: Multiscale phenomena in the tropical atmosphere over the western Pacific. *Mon. Wea. Rev.*, **120**, 407–430, https://doi.org/10.1175/1520-0493(1992)120<0407:MPITTA>2.0.CO;2.

Takahashi, H. G., H. Fujinami, T. Yasunari, and J. Matsumoto, 2010: Diurnal rainfall pattern observed by Tropical Rainfall Measuring Mission Precipitation Radar (TRMM-PR) around the Indochina peninsula. *J. Geophys. Res.*, **115**, D07109, https://doi.org/10.1029/2009JD012155.

Takahashi, T., 1978: Riming electrification as a charge generation mechanism in thunderstorms. *J. Atmos. Sci.*, **35**, 1536–1548, https://doi.org/10.1175/1520-0469(1978)035<1536:REAACG>2.0.CO;2.

Thornton, J. A., K. S. Virts, R. H. Holzworth, and T. P. Mitchell, 2017: Lightning enhancement over major oceanic shipping lanes. *Geophys. Res. Lett.*, **44**, 9102–9111, https://doi.org/10.1002/2017GL074982.

Vincent, C. L., T. P. Lane, and M. C. Wheeler, 2016: A local index of Maritime Continent intraseasonal variability based on rain rates over the land and sea. *Geophys. Res. Lett.*, **43**, 9306–9314, https://doi.org/10.1002/2016GL069987.

Virts, K. S., and R. A. Houze, 2016: Seasonal and intraseasonal variability of mesoscale convective systems over the South Asian monsoon region. *J. Atmos. Sci.*, **73**, 4753–4774, https://doi.org/10.1175/JAS-D-16-0022.1.

——, J. M. Wallace, M. L. Hutchins, and R. H. Holzworth, 2013: Diurnal lightning variability over the Maritime Continent: Impact of low-level winds, cloudiness, and the MJO. *J. Atmos. Sci.*, **70**, 3128–3146, https://doi.org/10.1175/JAS-D-13-021.1.

Waliser, D. E., 2006: Intraseasonal variability. *The Asian Monsoon*, B. Wang, Ed., Springer, 203–258.

Wang, B., 2005: Theory. *Intraseasonal Variability in the Atmosphere–Ocean Climate System*, W. K. M. Lau and D. E. Waliser, Eds., Springer, 307–360.

——, 2006: *The Asian Monsoon*. Springer, 787 pp.

——, and X. Xie, 1997: A model for boreal summer intraseasonal oscillation. *J. Atmos. Sci.*, **54**, 72–86, https://doi.org/10.1175/1520-0469(1997)054<0072:AMFTBS>2.0.CO;2.

JOBNAME: JCLI 00#00 2021 PAGE: 18 SESS: 8 OUTPUT: Tue Apr 6 06:10:24 2021 Total No. of Pages: 18
/ams/jcli/0/jcliD200308

Wang, S., D. Ma, A. H. Sobel, and M. K. Tippett, 2018: Propagation characteristics of BSISO indices. *Geophys. Res. Lett.*, **45**, 3420–3429, https://doi.org/10.1029/2018GL078321.

Xie, S., H. Xu, N. Saji, Y. Wang, and W. T. Liu, 2006: Role of narrow mountains in large-scale organization of Asian monsoon convection. *J. Climate*, **19**, 3420–3429, https://doi.org/10.1175/JCLI3777.1.

Xu, W., and S. A. Rutledge, 2018: Convective variability associated with the boreal summer intraseasonal oscillation in the South China Sea region. *J. Climate*, **31**, 7363–7383, https://doi.org/10.1175/JCLI-D-18-0091.1.

——, E. J. Zipser, Y. Chen, C. Liu, Y. Liou, W. Lee, and B. Jong-Dao Jou, 2012: An orography-associated extreme rainfall event during TiMREX: Initiation, storm evolution, and maintenance. *Mon. Wea. Rev.*, **140**, 2555–2574, https://doi.org/10.1175/MWR-D-11-00208.1.

Yokoi, S., S. Mori, M. Katsumata, B. Geng, K. Yasunaga, F. Syamsudin, Nurhayati, and K. Yoneyama, 2017: Diurnal cycle of precipitation observed in the western coastal area of Sumatra Island: Offshore preconditioning by gravity waves. *Mon. Wea. Rev.*, **145**, 3745–3761, https://doi.org/10.1175/MWR-D-16-0468.1.